Dry friction between flat surfaces: multistable elasticity vs. material transfer and plastic deformation

M.H. Müser

Institut für Physik, Johannes Gutenberg-Universität, 55099 Mainz, Germany
E-mail: martin.mueser@uni-mainz.de

A generic model for frictional forces between two monoatomic crystals is investigated by molecular dynamics simulations. Two solids, each composed of several atomic layers, are brought into contact and moved against each other. The mechanisms that lead to finite pinning (static friction) forces are analyzed by varying the geometry, the interfacial interaction, and the externally applied force. Material transfer leading to welded junctions is seen to be responsible for friction between strongly adhering surfaces. Chemically passivated surfaces pin if they deform plastically. In no region of the model's parameter range can finite frictional forces be attributed to multistable elasticity. Such wearless pinning mechanisms play the predominant role in Frenkel–Kontorova and Tomlinson models. In the parameter range where pinning is observed, externally driven sliding induces wear at the interface.

KEY WORDS: friction; Frenkel–Kontorova model; material transfer; plastic deformation; molecular dynamics

1. Introduction

Why should two flat crystalline surfaces placed on top of one another resist lateral motion? The answer to this question is less obvious than one might think. Starting from a description where the two crystals are interpreted as rigid units, a finite shear resisting force (per surface atom) can only be found if the two surfaces are commensurate (share common periodicities within the interface). Commensurability, however, is an unusual condition. Even completely identical surfaces are incommensurate, unless they are perfectly oriented with respect to one another. In the following discussion, it will be assumed that the two surfaces are incommensurate. The Tomlinson model [1], the Frenkel–Kontorova model [2,3], and related theories [4,5] all show that two incommensurate surfaces may have finite friction if the compliance of at least one crystal exceeds a threshold value. The threshold value depends on the way in which incommensurability is achieved and on how strong the interactions between the surfaces are [3,5]. Once the compliances or the interfacial interactions are large enough for surface atoms to deflect sufficiently from their equilibrium sites, many mechanically stable atomic configurations exist for any given relative position and orientation of the two crystals. This multistable elasticity ultimately leads to pinning between the surfaces of two solids resulting in finite shear forces and finite friction.

Recent theoretical [6] and numerical [7,8] analyses based on explicit atom–atom potentials suggest that this pinning mechanism is not efficient, which is the reason why multistable elasticity does not explain the ubiquitous existence of friction. Flat crystalline surfaces of noble and transition metals are unlikely to pin, as shown by Hirano and Shinjo [6]. Sørensen et al. obtained non-zero average lateral forces between a pyramidal copper tip and a flat crystalline copper surface provided that the systems were commensurate or if

the surface of the tip was extremely small [7]. In the latter case, the frictional forces were related to wear rather than to elastic deformations. Müser and Robbins showed that the interaction between atoms that lie on opposing sides of a sliding incommensurate interface have to be much stronger than those within the crystals in order to pin two elastically deformable crystals [8]. Their study, however, omitted long-range elastic deformations as well as material transfer and plastic deformations, because atoms in the bulk were coupled harmonically to their lattice sites.

The focus of the present computer simulation study is to analyze under which circumstances pinning of two dry, crystalline surfaces can be attributed to multistable elasticity and at what point other friction mechanisms start to be predominant. The two important alternative friction mechanisms are expected to be plastic deformation for chemically passivated surfaces and welding of the junction provided that the surfaces are strongly adhesive. The first mechanism becomes important if the contact pressure exceeds the penetration hardness of at least one of the two solids, while the latter mechanism incorporates material transfer between the two solids.

In order to account for all three friction mechanisms, long-range elasticity, material transfer, and plastic deformation must be made possible in the simulation. In the present study, the effect of long-range elasticity is taken into account by adding more and more explicitly treated crystalline layers in each wall. Only atoms in an outermost layer are coupled harmonically to their ideal lattice positions. All other atoms are unconstrained. This implicitly allows for material transfer across the interface. The adhesive strength between the surfaces is modeled by increasing the (attractive) forces between unlike atoms. In the initial configurations, atoms on either side of the interface are identical, while atoms on different side of the interface are unlike. As the interfacial in-

teratomic forces become larger than the forces between like atoms, the initial configuration becomes thermodynamically metastable and ultimately unstable. This instability gives a natural limit to the applicability of the wearless pinning mechanism through elastic deformation.

It is worth pointing out that it is by no means desirable to base the calculations on interfacial strengths that correspond to typical experimental values. E.g., if there is only a *small* interaction asymmetry in the real system which favors material mixing and cold welding of the junction, then mixing and welding will take place on a time scale that may be from μs up to several months. The typical time scale of a computer simulation, however, is only a few nanoseconds. Thus, in order to study qualitatively the tribological side effects of cold welding, one has to enhance the mixing process. This can easily be done by magnifying the interaction asymmetry artificially, resulting in a reduced activation barrier for the mixing process. This simple trick thus makes it possible to bridge indirectly several orders of magnitude in time scales between experiment and simulation.

Plastic deformation is made possible by placing pyramids on top of the outermost layers rather than filling out the space completely with full layers. The use of pyramids will be limited to the study of chemically passivated surfaces. Chemical passivation is modeled by using purely repulsive interactions across the interface.

A computer simulation, partially similar in spirit to this study, has been done by Glosli and McClelland [9]. Two ordered monolayers of dense alkane chains were bound to *commensurate* walls and the interfacial interaction strength between the surfaces was varied. A transition from finite to vanishing friction was reported for weak interfacial strengths. As discussed in [8], such a transition to zero-shear forces is always a finite-size artifact for commensurate walls. Pinning between commensurate walls is a geometric effect and does not require multistable elasticity, plastic deformation, or material transfer. Hence, in order to analyze the relevance of the latter mechanisms, a completely new study has to be done where commensurability is avoided.

It should be stressed that this study focuses on *dry* friction, that is to say, no *initial* third bodies are present in the interface. So-called "third-bodies" can have serious implications on wear and fatigue [10], but even without invoking wear, "between"-sorbed atoms and molecules automatically lead to pinning and finite friction between incommensurate crystals [8,11].

The most sensitive way to determine whether or not a system is pinned, is to analyze its thermal motion. If the system is pinned in the thermodynamic limit, a *finite* version of the system will show activated diffusion, e.g., there is a subdiffusive regime [8]. Alternatively, one may say that a large system will effectively be pinned if a small system shows subdiffusive behavior, even though, strictly speaking, it is not pinned at infinite times. In many cases, however, the diffusion is so slow that during the time window accessible to the simulation, only small oscillations around an equilibrium position take place. Hence, the system can be considered pinned. It is able to withstand an externally applied force that does not exceed the static friction force. In much the same way, an experimentalist does not detect thermally activated diffusion or zero pinning forces if the interface is large enough. This comment also applies to situations where a large contact can be subdivided into smaller (yet large enough) subblocks that interact via weak elastic interactions, such as in the Burridge–Knopoff model [12].

2. Model

The model used in this study consists of two fcc crystals with [111] surfaces. Each crystal is composed of $l = 2, \ldots, 6$ [111] planes. The interactions between all atoms are Lennard-Jones (LJ) potentials

$$V = \sum_{i<j} 4\varepsilon_{ij}\big[(\sigma_{ij}/r_{ij})^{12} - (\sigma_{ij}/r_{ij})^6\big] + V_{\mathrm{c}}, \qquad (1)$$

with r_{ij} the distance between particles i and j, ε_{ij}, σ_{ij} the LJ interaction parameters, and V_{c} the bias potential, which makes V a continuous function at the cutoff radius r_{c} [13]. All units will be expressed in LJ units ε_0, σ_0, and the mass of an individual atom m_0, e.g., the unit of time is $t_0 = (m_0\sigma_0^2/\varepsilon_0)^{1/2}$. Only atoms within an outermost layer interact differently. Every atom in such a layer is coupled harmonically to its ideal lattice site with a coupling $\kappa = 400\varepsilon_0/\sigma_0^2$. No direct interaction is considered between two atoms belonging to the same outermost layer (Tomlinson model). The outermost layer of the top wall is allowed to move, while the center-of-mass of the outermost layer of the bottom wall is kept fixed. The distance between two adjacent lattice sites is chosen such that the total energy of a perfect fcc crystal would be minimized, which ensures reasonable lattice constants. Choosing the distance between two adjacent lattice sites such that the free energy is minimized yields similar results.

The interaction strength between like atoms (atoms originating from the same side of the interface) is ε_0, while unlike atoms (atoms originating from opposing sides of the interface) interact with variable strength ε_1. The atoms retain their interactions after material exchange. Two geometries are investigated. (i) *Rotationally incommensurate surfaces.* The [111] layers correspond to a triangular lattice with a six-fold symmetry axis. If one wall is rotated by 90°, the walls are incommensurate. In order to achieve a quadratic shape, $N = 17 \times 20$ atoms are used per layer and one axis is slightly compressed. The final size of the surface is $(18.275\sigma_0)^2$. (ii) *Compressionally incommensurate surfaces.* The bottom wall consists of $N = 16 \times 16$ atoms and a surface of $17.2 \times 14.9\sigma_0^2$. The top wall is orientationally perfectly aligned, but it contains $N = 18 \times 18$ atoms. In order to account for the compression in the upper wall, the LJ interaction length in the upper wall is altered to $\sigma'' = 8\sigma_0/9$. This choice of σ'' ensures that the stress tensor is similar for both crystals. The LJ interaction length for interaction between

atoms originating from different sides of the interface is chosen to be $\sigma' = (\sigma'' + \sigma_0)/2$. Strictly speaking, neither case is truely incommensurate. Using periodic boundary conditions makes incommensurability impossible. However, the degree of commensurability is so small that the systems behave as if they were incommensurate.

All simulations are done at low temperatures, namely $k_B T = 0.1\varepsilon_0$. The top wall's center-of-mass is force free in the lateral direction unless otherwise mentioned. The normal force or load L is constant throughout each simulation. There are no constant-separation or constant-velocity constraints. If free diffusion of the top wall is observed (without signs of a subdiffusive regime), an upper bound for the pinning free energy per atom $\Delta F_{\text{bound}} = 0.003\varepsilon_0$ can be given. This estimation is based on the cautious assumption that subdiffusive behavior becomes obvious for $N \Delta F_{\text{bound}}/k_B T = 5$ and the values of N and $k_B T$ specified above. Such small values of ΔF_{bound} would result in extremely low friction coefficients, especially for the normal loads considered below. To be specific, for the given choices of normal loads, system sizes, and temperatures, it is possible to see pinning if the friction force is as small as $0.001L$. In most simulations, the system is kept at constant temperature by adding a damping force proportional to velocity and damping coefficient γ as well as a random force to each atom [14]. This creates partially non-deterministic, diffusive dynamics, which are acceptable, because the simulations aim to determine potential barriers rather than realistic dynamics. It is even desired to incorporate randomness into the trajectories as this makes possible to observe diffusion in an efficient way. The one-dimensional diffusion coefficient $D_0^{(l)}$ of an unpinned system (e.g., a system coupled to a thermostat and diffusing on a perfectly flat wall) can be given by

$$D_0^{(l)} = k_B T/\gamma l N m_0, \qquad (2)$$

where l gives the number of layers and N the number of atoms per layer. The real diffusion coefficient D is calculated by exploiting the relationship between D and the mean-square displacement,

$$D = \frac{1}{2} \lim_{t \to \infty} \frac{\partial}{\partial t} \langle [X(t) - X(0)]^2 \rangle, \qquad (3)$$

with $X(t)$ the x-coordinate of the top wall at time t. D is evaluated typically at times $t = 50t_0$ rather than taking $t \to \infty$ and the correlation function $\langle [X(t) - X(0)]^2 \rangle$ is usually averaged over $750t_0$, which corresponds to 1.5×10^5 molecular dynamics steps.

Once a system is pinned, D tends to zero and it is possible to calculate a non-zero static friction force F_s, which is defined as the minimum lateral force needed to initiate sliding. F_s is calculated by applying a lateral force $F_x(t)$ that slowly increases with time. As $F_x(t)$ exceeds F_s, the top wall shows a rather abrupt transition from the regime where the response of the upper wall to F_x is elastic to the sliding regime. (See, e.g., figure 7.)

3. Results

3.1. Strongly adhering surfaces

Strongly adhering surfaces are modeled by using a cut-off radius $r_c = 1.7\sigma$ for all interactions, independent of the atom species. Thus, in an fcc solid, interactions with nearest neighbors and next nearest neighbors would be treated explicitly, while interactions with atoms further apart would be neglected. Choosing a larger value for r_c would alter the results insignificantly for the present purposes, while the computation time would increase considerably.

The initial normal adhesive pressure between the crystal is in the order of ε_1/σ_0^3. A normal load of $2\varepsilon_0/\sigma_0$ is added to the intrinsic adhesive load onto each atom in the outermost top wall layer. Note that the conversion between pressures and forces per atom is about unity using Lennard-Jones units. As the interfacial interaction strength ε_1 exceeds ε_0, the initial condition of two perfect crystals in contact will be thermodynamically metastable or unstable, because energy can be gained if two atoms from different crystals swap their position. In the long run, mixing will occur. This effect makes physical properties of the system time-dependent. E.g., the correlation function $\langle [X(t) - X(0)]^2 \rangle$ will be quantitatively different before and after mixing. It turns out that there is a relatively well-defined boundary between values of $\varepsilon_1/\varepsilon_0$, where material transfer happens spontaneously and those where the unmixed metastable states are long-lived. Examples are shown in figures 1 and 2 for $l = 2$ layers per wall. While basically no mixing occurred within $10t_0$ for $\varepsilon_1/\varepsilon_0 = 8$ (figure 1), strong mixing occurred in the same time span for $\varepsilon_1/\varepsilon_0 = 10$ (figure 2). In both cases, unmixed initial configurations were chosen.
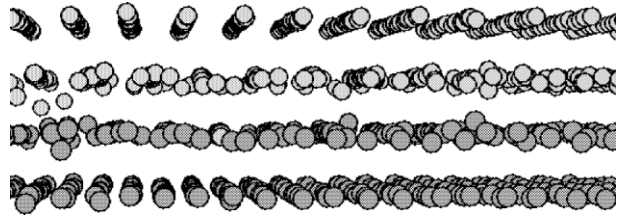

Figure 1. Part of configurations after the rotationally incommensurate system (two layers per wall) underwent free diffusion for a time $t = 10t_0$. Dark atoms originate from the lower wall, light atoms originate from the upper wall. Interaction strength across the interface relative to intrabulk interaction, $\varepsilon_1/\varepsilon_0 = 8$.
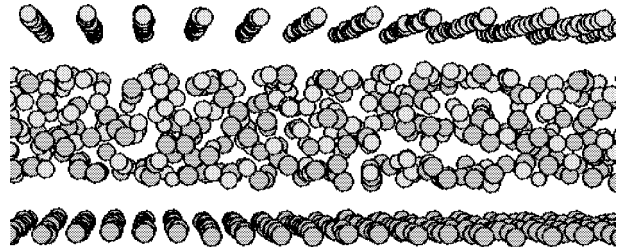

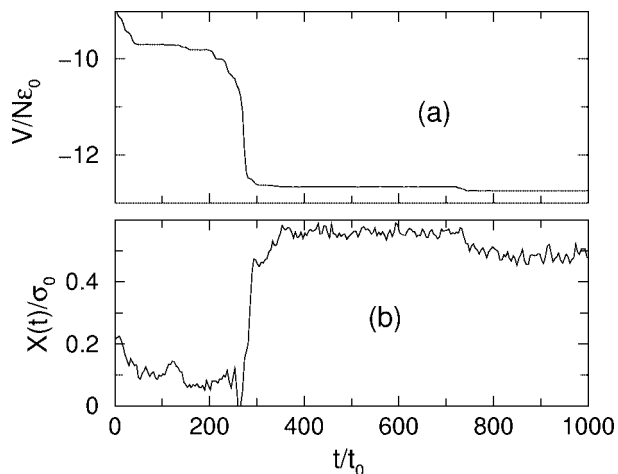Figure 2. Same as previous figure, but $\varepsilon_1/\varepsilon_0 = 10$.

Figure 3. (a) Potential energy V/N per particle and (b) x-coordinate of top wall as a function of time for compressionally incommensurate surfaces and strong interfacial interactions $\varepsilon_1/\varepsilon_0 = 10$. Initial conditions at $t = 0$ are two perfect fcc crystals in contact.
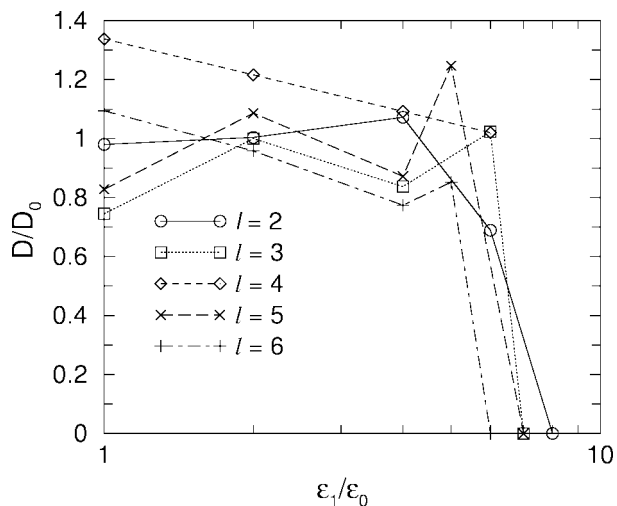

Figure 4. Diffusion constant D in units of the free-diffusion constant D_0 as a function of the interfacial strength $\varepsilon_1/\varepsilon_0$. l gives the number of explicitly treated layers per wall (rotationally incommensurate walls). Errors are about 20% of the absolute value.

The value of $\varepsilon_1/\varepsilon_0$ where spontaneous mixing sets in depends weakly on the number of layers and on the way that incommensurability is realized. The two extreme values of $\varepsilon_1/\varepsilon_0$, above which spontaneous mixing happens are $\varepsilon_1/\varepsilon_0 \approx 6$ for the compressionally incommensurate system with $l = 6$ layers per wall and $\varepsilon_1/\varepsilon_0 \approx 9$ for the rotationally incommensurate geometry and $l = 2$. During the mixing process, the surfaces seem to diffuse against each other. Once the mixing process ceases, e.g., the potential energy stops drifting to lower values, the surfaces pin. This is illustrated in figure 3 for the compressionally incommensurate system with two layers. At times $t < 300t_0$, the energy relaxes and the top wall appears to be mobile. Then, the system is metastable and the junction is welded. This is apparent from the fluctuations of the top wall around an equilibrium position. At $t \approx 750t_0$, the junction welds further, which is indicated by a tiny reduction in the potential energy. After this relaxation process is finished, the equilibrium position of the top wall has shifted slightly.

The relation of these mixing processes to real experiments deserves some attention. The value of $\varepsilon_1/\varepsilon_0$ where spontaneous mixing is seen in these computer simulations is certainly much larger than in experiments, where "spontaneous" might mean, let's say, "within one second". Hence, in order to invoke the mixing process without imposing artificial side conditions, we have to exaggerate the interfacial interaction strength, which moves the mixing process to smaller time scales. Once a system is mixed and pinned in the simulation, the frictional forces depend surprisingly little on $\varepsilon_1/\varepsilon_0$. We can therefore expect that mixing and welding occur qualitatively similar in real experiment in cases that could be characterized by $\varepsilon_1/\varepsilon_0$ just slightly above one.

In the regime where no spontaneous mixing occurs, the definition of a diffusion coefficient D such as in equation (3) is meaningful. Figure 4 shows D as a function of the relative interfacial interaction strength $\varepsilon_1/\varepsilon_0$. Once mixing occurs, the junction welds and D can be set to zero. There has

been no single case of pinning for both symmetries, compressionally incommensurate and rotationally incommensurate, where pinning has been observed in the absence of material transfer. In all cases where material transfer has been observed on the other hand, the junction was clearly pinned after the relaxation process had seized. The strength of the interfacial interaction strength where material transfer (and thus pinning) sets in are very close for the two symmetries studied. Hence, a disordered system such as the one represented in figure 2 will lead to static frictional forces while a layered, unmixed system is superlubric, i.e., only a small drag force similar to a Stokes friction force resists externally induced sliding. This last observation is a counterexample to previous simulation studies [15] where layering of confined fluids leads to a strong decrease in the diffusion of the confined liquid and thus to an enhanced friction between the confining solids.

The statements made above imply the conclusion that no pinning can be found for $\varepsilon_1/\varepsilon_0 \leqslant 1$, which would correspond to pinning of a thermodynamically stable system. These results show that wearless pinning or finite shear forces between two flat adhering crystalline Lennard-Jones surfaces is unlikely. A contribution to finite friction forces would only come from those regions that are (nearly) commensurate. Thus, in order to obtain a meaningful friction coefficient in a simulation, one would have to average over all possible relative orientations of the two surfaces. The results obtained here suggest that only a narrow region of relative orientations would contribute to the friction coefficient μ_s even if the surfaces were chemically identical. Thus the net (macroscopic) friction coefficients would be extremely small if multistable elasticity were the major contribution to frictional forces, in particular as a typical value for μ_s obtained in simulations of dry, commensurate interfaces is only ~ 0.3.

3.2. Chemically passivated surfaces

Chemical passivation is modeled by cutting off the interaction at the minimum of the Lennard-Jones potential. Thus, two non-chemically interacting atoms only repel but do not adhere. The short cutoff radius is applied only to atoms originating from different crystals, while the long-range interactions are still used for all other interactions. Consequently, the initial configurations with one atom species on one side of the interface and the other species on the other side of the interface is thermodynamically stable, no matter how large ε_1.

If the initial configuration is chosen to be similar to those in figure 1 (dense packing and periodic boundary conditions in the plane), no pinning of the surfaces can be seen, even if the normal load per area goes up to $L/A = 50\varepsilon_0/\sigma_0^3$, where a real crystal would yield. Increasing the interfacial strengths up to values of $\varepsilon_1/\varepsilon_0 = 16$ does not change the situation. At this value of $\varepsilon_1/\varepsilon_0$, adhering surfaces pin at zero normal load.

This observation suggests that finite shear forces can only occur if the chemically passivated surfaces deform plastically. In order to make plastic deformation possible, new initial conditions must be chosen such that the crystal has the possibility to yield, e.g., by placing pyramids on the outermost layers instead of full layers. An initial configuration for the rotational incommensurate surfaces and $l = 4$ layers per wall is shown in figure 5. The asperities used in this study fill out about 90% of the outermost layer's surfaces. This geometry might still artificially raise the threshold value for plastic deformation, but such details are not important while investigating qualitative features.

It is possible to classify the plastic deformation roughly into three regimes. For small loads, no reconstruction is observed within the time window of the simulation. At normal pressures $L/A \approx 6\varepsilon_0/\sigma_0^3$, small atomic rearrangements start to occur at the interface, while for loads $L/A > 12\varepsilon_0/\sigma_0^3$ major reconstructions of the asperities take place until the cavities shown in figure 5 are filled. Figure 6 shows a configuration after plastic deformation took place. A normal pressure of $L/A = 10\varepsilon_0/\sigma_0^3$ initiated the deformation. In the regimes where deformations take place, similar relaxation effects are seen as those shown in figure 3, in particular pinning (center-of-mass oscillations around a newly formed equilibrium site) after the relaxation process comes to a stop.

The systems are apparently pinned as soon as plastic deformation takes place. As long as they do not deform, the tendency to pin is extremely weak. Thermal fluctuations of the top wall around the equilibrium position are typically more than 10% of a lattice spacing. This fluctuation is relatively large considering the size of the contact area. The pinning can be related to a geometric effect, where the upper wall tries to minimize its gravitational energy. Sliding simulations (not presented below) give an estimate for the friction coefficient of less than 0.01 for this pinning mechanism.
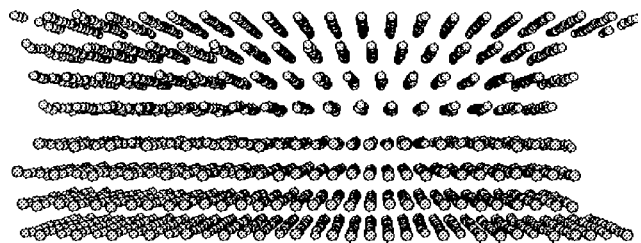

Figure 5. Initial configuration for chemically passivated surfaces with the possibility to yield under large normal loads. Both surfaces are identical fcc [111] surfaces but rotated by 90°.
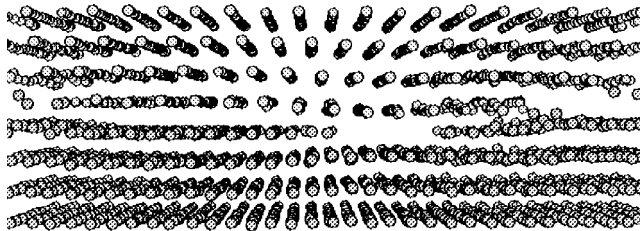

Figure 6. Same as figure 5, but after plastic deformation took place.

3.3. Retraction and sliding of pinned surfaces

All pinned systems of this study turned out to withstand an externally applied lateral force F_s per atom before sliding was initiated. According to Amontons' law, F_s is proportional to the load of the form L [16]. As shown in [11], this law is not only valid on a macroscopic scale but also for flat, microscopic contacts if the adhesive effects are included in the load. As a measure for the adhesive force L_{adh}, the contribution from the attractive part of the LJ interactions across the interface is taken. Alternatively, the retraction force L_{retr} is considered.

3.3.1. Strongly adhering surfaces

For strongly adhering surfaces, the L_{adh} and L_{retr} do not only depend on the interfacial interaction strength but also on the history of the contact. After mixing, retraction forces are larger and adhesive forces are smaller than before mixing. As a rule of thumb, one may say, however, that L_{retr} per surface element is close to ε_0 and L_{adh} is close to ε_1. Frictional forces depend very much on the history of the junction than L_{adh} and L_{retr}. This is particularly true for the initial configuration where mixing effects are just about to set in. An example is shown in figure 1, where only a few pairs of atoms exchanged between upper and lower crystal. Once a shear force is applied, the aging of the junction is enhanced and more mixing occurs. This aging is yet another indication that the friction mechanism is not wear free as in models based on multistable elasticity.

Exemplarily, we want to discuss the sliding of a system in which each wall contains six layers of atoms. An external normal pressure of $L/A = 2\varepsilon_0/\sigma_0^3$ is applied to the top wall and the interfacial interaction strength is chosen to $\varepsilon_1/\varepsilon_0 = 6$. The large value for the cutoff radius is employed. Retracting the top wall required a (negative) load per surface of $-L_{adh}/A \approx 2.4\varepsilon_0/\sigma_0^3$. A time-dependent shear force
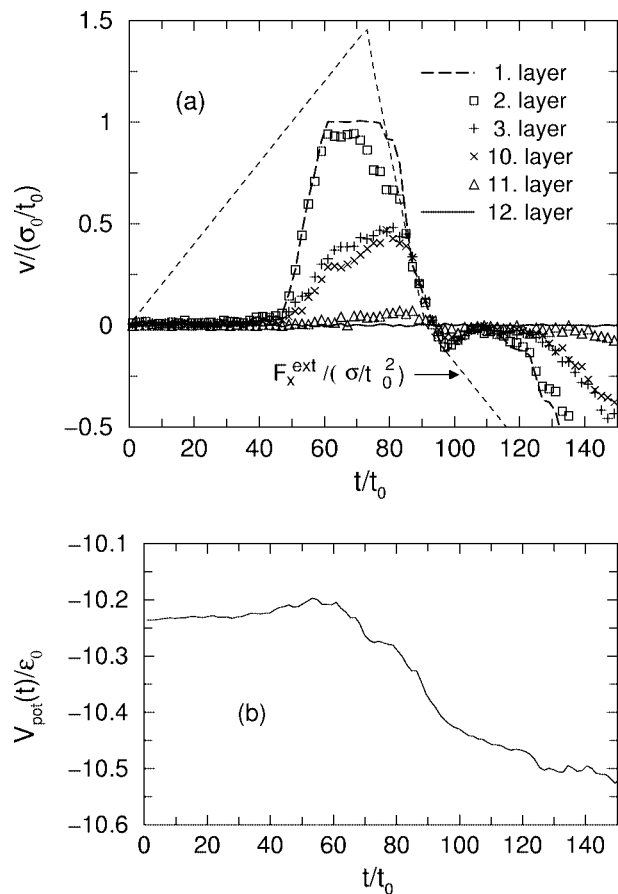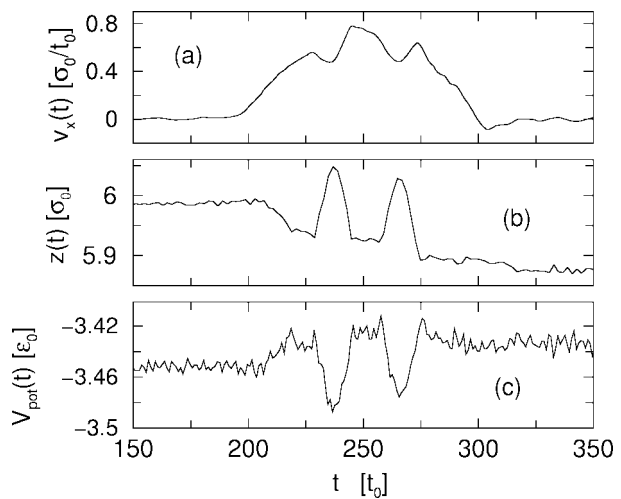
Figure 8. (a) Velocity of top wall $v_x(t)$ in pulling direction, (b) lateral position $z(t)$ of the top wall and (c) net interatomic potential energy per particle $V_{pot}(t)$ as a function of time.

ergy decreases as a function of time. Similar effects can be seen for subsequent depinning events as well. Once the junction ceases to slide, aging (decreasing potential energy with time) is slowed down significantly. Even after 20 pinning–depinning events (total of 2×10^6 MD steps), no final steady state could be observed.

3.3.2. Chemically passivated surfaces

For chemically passivated surfaces, retraction of the upper wall can be done at a nominally zero pulling force. Thus adhesive effects can be neglected in the effective load. As mentioned in secion 3.2, pinning only occurs after plastic deformation takes place. Due to the large surface coverage of the initial ridge that was chosen in this study and due to periodic boundary conditions, there is only a small load regime in which surfaces deform plastically, but do not yet fill out the space completely.

As an example of a sliding simulation, we want to focus again on a system consisting of four layers per wall with initial conditions similar to figure 6. The case of a normal pressure of $L/A = 8\varepsilon_0/\sigma_0^3$ is considered. For this value of the normal load, the surfaces deform plastically, yet, the newly formed ridges do not fill out the space completely. Details of the sliding simulation, which was done in a way similar to the one discussed in section 3.3.1, are shown in figure 8.

From figure 8(a), it can be concluded that the system depins at a time $t \approx 195t_0$. At this time, the value for the externally applied shear pressure $F_x(t)/A$ is about $0.15\varepsilon_0/\sigma^3$ (not shown here). This value would result in a relatively small friction coefficient of $\mu_s \approx 0.02$. This value of μ_s is reproduced by subsequent pinning–depinning events. Two features in figure 8 are worth special attention. (i) With each pinning–depinning event, the interatomic potential energy slightly increases, while the spacing becomes smaller. The decreased "gravitational" potential energy of the load overcompensates the deformation energy of the solid. (ii) At

Figure 7. (a) Average velocity per layer as a function of time. First layer corresponds to top wall, twelfth layer to bottom wall (original configuration has six layers per wall). The externally applied force F_x^{ext} corresponds to the dashed, triangular shaped line. The maximum velocity of the top wall's center-of-mass is artificially limited to $1\sigma_0/t_0$. (b) Net potential energy per particle during the first force-ramp cycle.

$F_x(t)$, shown in figure 7(a), was applied to the original (un-retracted) system in order to initiate sliding.

The velocities of top and bottom wall as well as of some representative layers are shown in figure 7(a) as a function of time. One atom is counted to belong to a certain layer l if its z-component of the coordinate falls into a suitably defined range $z_{min}^{(l)} \leqslant z < z_{max}^{(l)}$, with l independent ranges $z_{max}^{(l)} - z_{min}^{(l)}$. From the motion of the top wall, it is obvious that depinning takes place at a time $t \approx 45t_0$. At this time the friction force per atom in the outermost top wall layer is about $F_x \approx 0.75\varepsilon_0/\sigma_0$, which corresponds to about 0.4 times the externally applied load L. In this particular depinning event, one layer of atoms seems to stick to each outermost layer and two real sliding interfaces occur between the second and the third layer and the tenth and the eleventh layer.

The time-dependence of the net potential energy per particle, shown in figure 7(b) shows particularly interesting features. Before depinning, the potential energy has the tendency to increase with time. This increase can be related to the increase of elastic energy in the junction. Once the junction depins, strong mixing occurs and the potential en-

times $t \approx 230t_0$ and $t \approx 270t_0$, the two asperities are placed right on top of one another, which can be seen by their large vertical separation in figure 8(b). As the interaction across the interface is purely repulsive, the interfacial energy is minimum while the contact area is minimum, resulting in the minima of the net interatomic potential energy V_{pot}, as shown in figure 8(c). At the same time, the sliding velocity goes down as the upper wall "climbs" up the asperity at $t \approx 230t_0$, but the sliding velocity picks back up as it slides down the asperity at $t \approx 240t_0$. This effect, which we can understand from a purely geometric point of view, would not have been observable if the simulations had been done at constant separation. It would have been more likely to see strong abrasion of the asperities as reported in previous computer simulation studies employing fixed-separation constraints [17].

4. Conclusion and discussion

This study rules out the possibility that models like the Frenkel–Kontorova or the Tomlinson model can be used in their original form to explain why dry crystalline surfaces show friction when they are slid against each other. The reason is that two crystalline surfaces are nearly always incommensurate and interfacial interactions are usually too weak to dominate the forces within the bulk. As a consequence, the elastic deformations within the surface layers are too small in order to pin the two solids. For the Lennard-Jones solids investigated in this study, no parameter range could be found where two surfaces pinned via elastic deformations. No atomistically detailed simulation of two three-dimensional crystals in sliding motion is known to the author where wearless friction between two solids was observed, unless the solids were commensurate. Even adsorbed rare gas monolayers on noble metals are often not compliant enough to lock into the periodicity of the substrate [18,19], despite the fact that stabilization of the intrinsic periodicity through the bulk is absent in monolayers.

In this study, strongly adhesive solids pinned *after* material transfer occurred between the crystals. Chemically passivated surfaces (modeled by short-range interactions for atoms originating from different surfaces) pin only if there is the possibility for plastic deformation. The observation that wearless friction between unaligned MoS_2 crystals is extremely low in ultrahigh vacuum [20], should therefore not be an exception but rather the rule. The rapid raise of friction with exposure to air shows that friction between flat surfaces is presumably related to physisorbed atoms and molecules as suggested by He et al. [11].

Of course, a different class of potential might result in larger ranges where pinning of bare crystalline surfaces occurs through elastic deformation. Using Morse potentials, $V = \varepsilon[1 - \exp\{-a(r - r_0)\}]^2 - \varepsilon$, or more realistic potentials would make it possible to vary the bulk modulus independently of the cohesion energy. (For a Lennard-Jones (LJ) system, the bulk modulus and the cohesive energy (or

the energy to create a certain type of defect) are not independent properties, because no dimensionless parameter can be constructed from LJ parameters.) The ratio $\varepsilon_1/\varepsilon_0$ where pinning would occur (if a similar study were done but based on Morse potentials) will depend on the dimensionless variable ar_0. Small values of ar_0, resulting in soft solids, can be expected to show pinning at "small" values of $\varepsilon_1/\varepsilon_0$. However, a preliminary analysis shows that the region where pinning through elastic multistability occurs is not increased if reasonable values are taken for ar_0.

It is not the intention of this article to invalidate the Tomlinson, the Frenkel–Kontorova and related models in the context of friction. They are the only promising theories to date which develop simultaneously an analytical and microscopic understanding for many aspects of friction such as slip–stick. However, generalizations of these theories have to be considered when addressing the question of why friction between sliding objects is usually observed. Considering finite chains of molecules [21] or even individual atoms [22] between stiff or compliant solids will presumably result in tribological properties that are similar for commensurate and incommensurate systems. Also a phenomenological interpretation of the free parameters in the Tomlinson model as done recently by Baumberger and Caroli [23] yields understanding of many dynamical, tribological phenomena, even though the atomistic origin of some parameters remains obscure.

Acknowledgement

References

[1] G.A. Tomlinson, Phil. Mag. Series 7 (1929) 905.
[2] Y.I. Frenkel and T. Kontorova, Zh. Eksp. Teor. Fiz. 8 (1938) 1340.
[3] P. Bak, Rep. Progr. Phys. 45 (1982) 587.
[4] M. Weiss and F.-J. Elmer, Phys. Rev. B 53 (1996) 7539.
[5] M.O. Robbins and M.H. Müser, in: *Handbook of Modern Tribology*, ed. B. Bhushan (CRC Press, New York), and references therein, in press.
[6] M. Hirano and K. Shinjo, Phys. Rev. B 41 (1990) 11837.
[7] M.R. Sørensen, K.W. Jacobsen and P. Stoltze, Phys. Rev. B 53 (1996) 2101.
[8] M.H. Müser and M.O. Robbins, Phys. Rev. B 64 (2000) 2335.
[9] J.N. Glosli and G. McClelland, Phys. Rev. Lett. 70 (1993) 1960.
[10] I.L. Singer, MRS Bullet. 26 (1998) 37.
[11] G. He, M.H. Müser and M.O. Robbins, Science 284 (1990) 1650.
[12] R. Burridge and L. Knopoff, Bull. Seismol. Soc. Am. 57 (1967) 341.
[13] M.P. Allen and D.J. Tildesley, *Computer Simulation of Liquids* (Clarendon Press, Oxford, 1987).
[14] K. Kremer and G.S. Grest, J. Chem. Phys. 92 (1990) 5057.
[15] J. Gao, W.D. Luedtke and U. Landman, Phys. Rev. Lett. 79 (1997) 705.
[16] F.P. Bowden and D. Tabor, *The Friction and Lubrication of Solids* (Clarendon Press, Oxford, 1986);
B.N.J. Persson, *Sliding Friction* (Springer, Berlin, 1998).

[17] J. Gao, W.D. Luedtke and U. Landman, Science 270 (1995) 605;
     U. Landman, W.D. Luedtke and J. Gao, Langmuir 12 (1996) 4514.

[18] J. Krim, D.H. Solina and R. Chiarello, Phys. Rev. Lett. 66 (1991) 181;
     J. Krim and R. Chiarello, J. Vac. Sci. Technol. A 9 (1991) 2566.

[19] E.D. Smith, M.O. Robbins and M. Cieplak, Phys. Rev. B 54 (1996) 8252.

[20] J.M. Martin, C. Donnet, Th. Le Mogne and Th. Epicier, Phys. Rev. B 48 (1993) 10583.

[21] M.G. Rozman, M. Urbakh and J. Klafter, Europhys. Lett. 39 (1997) 183;
     M.G. Rozman, M. Urbakh, J. Klafter and F.-J. Elmer, J. Phys. Chem. B 102 (1998) 7924.

[22] M.G. Rozman, M. Urbakh and J. Klafter, Phys. Rev. E 57 (1998) 7340.

[23] T. Baumberger and C. Caroli, Eur. Phys. J. B 4 (1998) 13.